PET quantitation and imaging of the non-pure positron-emitting iodine isotope [124]I

H. Herzog[a],*, L. Tellmann[a], S.M. Qaim[b], S. Spellerberg[b], A. Schmid[a], H.H. Coenen[b]

[a] *Institute of Medicine, Forschungszentrum Jülich GmbH, D-52425 Jülich, Germany*
[b] *Institute of Nuclear Chemistry, Forschungszentrum Jülich GmbH, D-52425 Jülich, Germany*

Abstract

A series of PET studies using phantoms is presented to characterize the imaging and quantitative performance of the positron-emitting iodine isotope [124]I. Measurements were performed on the 2D-PET scanner GE 4096+ as well as on the Siemens PET scanner HR+ operated in both 2D and 3D modes. No specific correction was applied for the γ-rays emitted together with the positrons. As compared to ^{18}F, in studies with [124]I there is a small loss of image resolution and contrast, and an increase in background. The quantitative results varied between different scanners and various acquisition as well as reconstruction modes, with an average relative difference of $-6 \pm 13\%$ (mean $\pm$ SD) in respect of the phantom radioactivity as measured with γ-ray spectroscopy. We conclude that quantitation of a radiopharmaceutical labelled with [124]I is feasible and may be improved by the development of specific corrections. © 2002 Elsevier Science Ltd. All rights reserved.

Keywords: [124]I; PET imaging; PET quantitation

1. Introduction

The non-pure positron-emitting iodine isotope [124]I has been utilized in comparative studies in which diagnostic or therapeutic radiopharmaceuticals labelled with the ^{123}I or ^{131}I were characterized with the help of PET (Langen et al., 1990; Carnochan et al., 1994; Coenen et al., 1995; Pentlow et al., 1996). It should be pointed out that, on one hand, [124]I is not an ideal PET-isotope due to its low positron abundance of only 23% (ICRP Publication 38, 1983) and long half-life of 4.18 d, which leads to a high radiation dose. On the other hand, the long half-life is advantageous for developing radiochemical syntheses and allows the tracing of slow biochemical processes which cannot be adequately examined by the commonly used short-lived positron emitters such as ^{11}C or [18]F. Since the positrons emitted by [124]I have mean energies of <1 MeV, a severe degradation of image resolution, caused by long range positrons, need not be expected. There are, however, single photons with energies of 602 and 722 keV and abundance of 60% and 10%, respectively, which may result in additional random, scatter, and so-called gamma coincidences. Whereas the 602 keV photons are directly accepted within the discriminator energy window ranging from 350 to 650 keV, the 722 keV photons may be recorded only after having lost part of their energy by Compton scattering. As about 50% of the single gamma-photons are emitted in cascade with the positrons, such a photon may cause a gamma coincidence with one of the annihilation photons. The increase of non-true coincidences leads to a low-frequency background noise which results in lower image contrast. A high occurrence of non-true coincidences may become critical, especially in the case of 3D-PET where retracted septa do not hinder unwanted

*Corresponding author. Tel.: +49-2461-61-5913; fax: +49-2461-61-8310.

E-mail address: h.herzog@fz-juelich.de (H. Herzog).

coincidences on their way to the detector. The aim of this work is to investigate how [124]I is imaged in both qualitative and quantitative aspects using 2D- as well as 3D-PET. For the 2D-mode two different scanners were compared.

2. Materials and methods

2.1. Production of [124]I

[124]I was produced via the [124]Te(p, n) nuclear reaction on 99.8% enriched [124]TeO$_2$ using the proton energy range of 14→10 MeV (Scholten et al., 1995; Qaim et al., 1996). This nuclear reaction provides very high-purity [124]I, the levels of ^{125}I and [126]I being <0.01% (Bastian et al., 2001).

2.2. PET measurements and data analysis

For quantitative measurements a phantom was used consisting of two compartments roughly simulating the shape of the cerebral cortex and white matter at the level of the basal ganglia (Fig. 1). The phantom is a straight cylinder of 10 cm length so that measurements are independent of the location in the z direction (scanner's longitudinal axis) if the phantom's cross-section is oriented transaxially. The grey (cortex) and white matter chambers (GM and WM) with volumes of 627 and 508 ml, respectively, are shaped so that regions of interest (ROIs) can be placed without evoking a partial volume effect. In a first study (S1) about 35 MBq of [124]I were injected into the two chambers and in a second study (S2) about 18.5 MBq. To simulate the GM/WM radioactivity distribution in

Fig. 1. PET image of the brain-shaped two-chamber phantom filled with [124]I and scanned for 60 min with the HR+ in 3D-mode.

blood flow studies more radioactivity was put in the GM chamber, so that the GM/WM ratios of radio-activity concentration were 3.1:1 for S1 and 2.2:1 for S2. The amount of [124]I-radioactivity installed in the phantom was determined by measuring several samples via γ-ray spectroscopy.

In each study the phantom was first positioned in a GE/Scanditronix PET scanner PC 4096+ (Rota Kops et al., 1990) which operates exclusively in 2D-mode. A series of at least 6 emission scans with a frame duration of 10 min (S1) or 1 h (S2) was acquired. After these measurements the phantom was placed in the Siemens/CTI scanner HR+ (Brix et al., 1997) to obtain emission scans without and with retracted septa, i.e., in 2D- and 3D-mode. Each emission scan consisted of up to six frames, each with a duration of 10 min (S1) or 1 h (S2). In order to examine low count data and to check the linearity over time by deducing the half-life of [124]I from the acquired data, the measurements were repeated after 16 days in the case of S1 and after 11 days in the case of S2. In this way, early studies S1A and S2A and late studies S1B and S2B were available.

All transmission scans were performed over 20 min with the phantom already filled with radioactivity so that the measured attenuation correction was based on "warm" transmission data. "Cold" transmission data also became available by applying separate transmission scans during which the phantom was filled with water, but not with radioactivity. The exact repositioning with respect to emission scans was assured with the help of laser beams.

All emission data were corrected for measured attenuation as well as for random and scattered coincidences. For both scanners all corrections and reconstructions were applied with the standard settings used in research and clinical studies. For the PC4096+ random coincidences were estimated from the single count rates and for the HR+ randoms were derived using the delayed window approach and subtracted instantly during acquisition. With both PET systems the 2D-scatter correction was performed according to the convolution–subtraction method introduced by Bergström et al. (1983). The 3D-scatter correction of the HR+ was done alternatively with the sinogram- and image-based scatter approaches suggested by Watson et al. (1997); Watson (2000) and available in alternative reconstruction modes (see below) of the CTI–PET software package version 7.2. No attempt was made to correct for gamma coincidences as has recently been suggested for [76]Br (Lubberink et al., 2001). The corrected data were reconstructed with filtered back projection. When using the PC4096+ a Hann filter with a width of 4.5 mm was employed leading to a reconstructed image resolution (FWHM) of about 7 mm for ^{18}F as detailed previously (Rota Kops et al., 1990). In the case of the HR+ two reconstruction
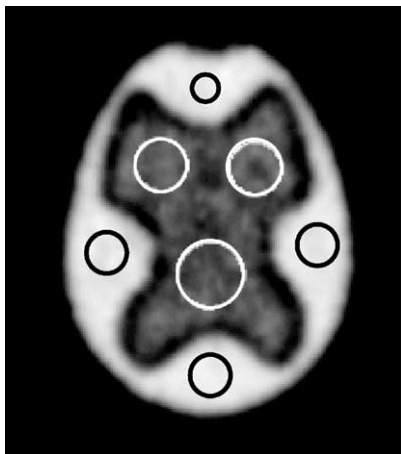
modes were applied, here referred to as VP-mode (vector processor based) and CPU-mode (workstation based) which are nearly equal for 2D data, but different for 3D. The older mode (VP) uses the fully 3D-filtered back-projection approach of PROMIS (Defrise et al., 1989) and the sinogram-based 3D-scatter correction (Watson et al., 1997), whereas the newer mode (CPU) first performs a Fourier-rebinning of the 3D-data (Defrise et al., 1997) which is followed by a conventional 2D-filtered backprojection. The CPU-mode utilizes the recent image-based scatter correction (Watson, 2000). The VP-based filtered backprojection involved a Hann filter with a cutoff frequency of 0.5 cycles/pixel and the CPU-version a Shepp filter with a width of 2.48 mm so that the reconstructed image resolution for ^{18}F was about 6 and 5.5 mm, respectively.

An equivalent series of measurements in both scanners was recorded with the two-chamber phantom filled with ^{18}F dissolved in water. Here, the amount of inserted radioactivity was determined from three 1 ml samples taken from the GM and WM chamber each. The samples were measured in a well counter, cross-calibrated to each of the two PET scanners.

The images of the two-chamber phantom were analysed by defining 6 circular ROIs with diameters between 12 and 34 mm in a plane at the axial middle of the phantom. Four ROIs were placed over the grey and three over the white matter area (Fig. 1). This was repeated in 4 adjacent image planes so that the mean radioactivity of each chamber could be read from 20 or 15 ROIs, respectively. Finally, GM/WM ratios were calculated and compared with the real ratios.

In addition, a glass capillary with an inner diameter of 1 mm, filled with either ^{124}I or ^{18}F, was partly inserted into a tube located in the central axis of a cylindrical phantom of 20 cm diameter filled with water. It was imaged in both scanners. The central axis of the phantom coincided with the scanner's longitudinal axis. Furthermore, the phantom was positioned within the field of view so that one half on the scanner's planes saw the capillary in air, whereas the other half saw it in water. In order to obtain line spread functions of the raw data, the sinograms of the capillary acquisitions were evaluated as follows. At least 10 adjacent horizontal lines of the 2D-sinograms were averaged after having adjusted the maxima of these projections to the same bin. Using these line spread functions the background caused by non-true coincidences could be judged for all conditions, i.e., ^{124}I, ^{18}F, 2D, 3D air, and water. To determine the image resolution, all recordings of the capillary were corrected and reconstructed as already described for the two-chamber phantom. Then horizontal and vertical line profiles were defined in four adjacent image planes so that the profiles crossed the maximum of the reconstructed point images. The reconstructed

image resolution expressed as FWHM was obtained with the help of Gaussian fits of these profiles. The reported results are averaged over all horizontal and vertical profiles.

To judge the imaging characteristics of ^{124}I in comparison to ^{18}F the two radionuclides were alternately injected into a 3D-Hoffman brain phantom filled with water and scanned with both scanners with standard brain protocols in 2D (PC4096 + and HR +) and 3D (HR +). The reconstruction was done as described above.

3. Results

When the capillary filled with either ^{124}I or ^{18}F was scanned with the HR + for the conditions 2D and 3D and each with air or water, normalized projections were obtained as shown in Fig. 2. Since these data were acquired with the HR +, they were already random corrected by the delayed window subtraction procedure. In 2D as well as in 3D there was a more than tenfold increase of background counts with ^{124}I compared to ^{18}F. In water, the background between ^{18}F and ^{124}I differed by a factor of only 5.5 and 2.5 for 2D and 3D, respectively. When the capillary was in water rather than in air the background was no longer uniform, but decreased with a greater radius.

When the PC4096 + and HR + 2D-acquisitions of the capillary filled with ^{18}F and located in water are compared (Fig. 3), the profiles found with the HR + show an increased background. This difference is more pronounced for ^{124}I. There was nearly no difference between the two scanners for ^{18}F as well as for ^{124}I when projections of the line source measured in air were evaluated.

Point spread images from line source data, which were reconstructed with the routinely used settings, yielded values of reconstructed image resolution expressed as FWHM as summarized in Table 1. For both scanners there is a slight deterioration of resolution of 0.5–1 mm when ^{124}I is used.

Attenuation correction utilizing a "warm" instead of a "cold" transmission scan gave a decrease of the reconstructed radioactivity concentration by 2 to 4%.

Fig. 4 displays all radioactivity concentrations obtained in S2A and S2B studies. For the HR +, the CPU-based data are shown. Relative differences in the radioactivity concentration of the GM chamber determined via PET and γ-ray-spectroscopic measurements are listed in Table 2. Several trends can be observed here. The HR + results are lower than those of the PC4096 +. For the HR +, the VP- and CPU-based reconstructions yielded similar findings in 2D, whereas in 3D the VP results are considerably lower. These trends are true for S1 as well as for S2, although there is
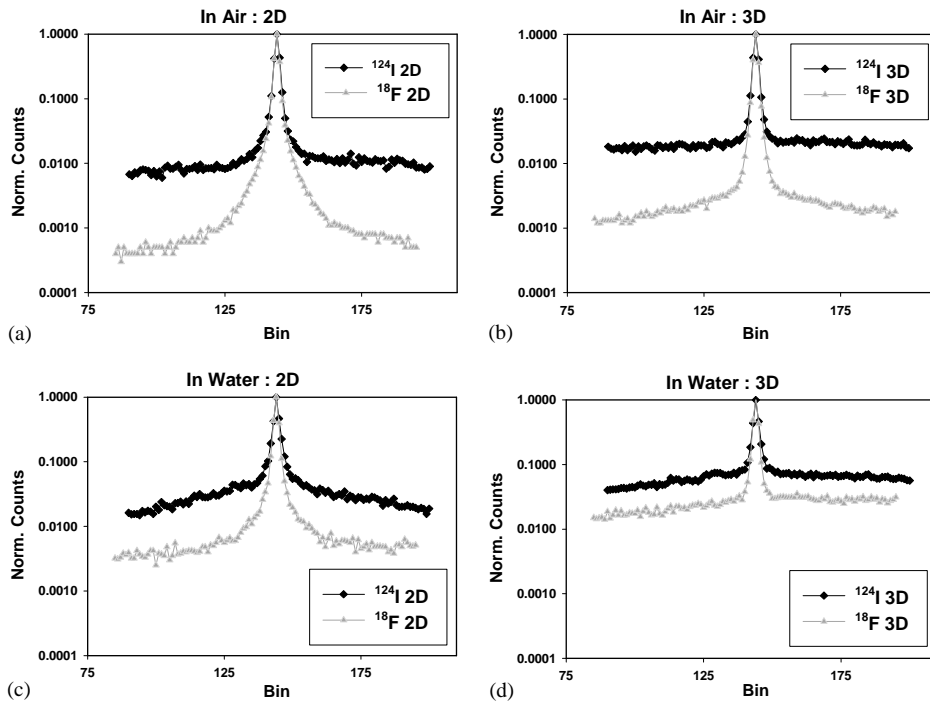
Fig. 2. Normalized profiles derived from transaxial sinograms of a line source filled with either [124]I or ^{18}F, positioned in air as well as in water. The sinograms were acquired in the 2D-and 3D-mode of the HR + .
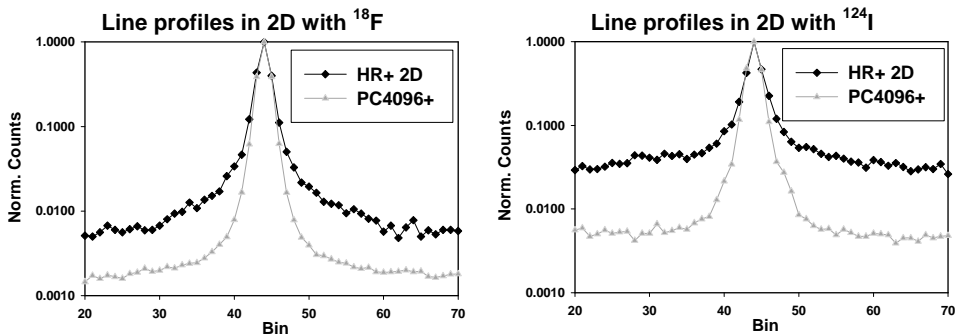
Fig. 3. Normalized profiles derived from transaxial sinograms of a line source filled with either [124]I or ^{18}F, positioned in water. All sinograms were acquired in the 2D-mode either with the PC4096 + or HR + .

a difference of 20–25% between S1 and S2. This general discrepancy may be best explained by a bias of the reference measurement, i.e. γ-ray spectroscopy. Furthermore, the differences observed within one study with the two scanners, and among the four modes of the HR + were also present when the phantom was filled with ^{18}F instead of [124]I.

The evaluation of the sinograms of all studies with the two-chamber phantom showed a background outside the phantom of up to 5% of the maximum count value for both ^{18}F and [124]I. After reconstruction, ROIs placed outside around the phantom had an average radio-activity of < 1% of the GM average for ^{18}F as well as

[124]I. These results were true for the PC4096 + and the HR + (2D and 3D).

The measurements SnA and SnB were about 4 and 3 half-lives of [124]I apart. Table 2 shows only some minor differences between the early and the late measurements. This fact is also confirmed when the half-life of [124]I was deduced from the measured data and compared with the literature value of 4.18 d. The relative differences between 4.18 d and the calculated half-lives were $-1.2 \pm 1.5\%$ within a range of –4.3–0.4%.

When the GM/WM of the two-chamber phantom was evaluated, differences between the early and the late scans became obvious (Table 3). The PC4096 + had a

Table 1
Reconstructed image resolution measured with line source in water (FWHM, in mm)

	Filter	[124]I	[18]F
PC4096+	Hann 4.5 mm	8.0	7.5
HR+2D	Shepp 2.48 mm	6.3	5.5
HR+3D	Shepp 2.48 mm	6.1	5.1

ß⁺-radioactivity of [124]I measured via PET
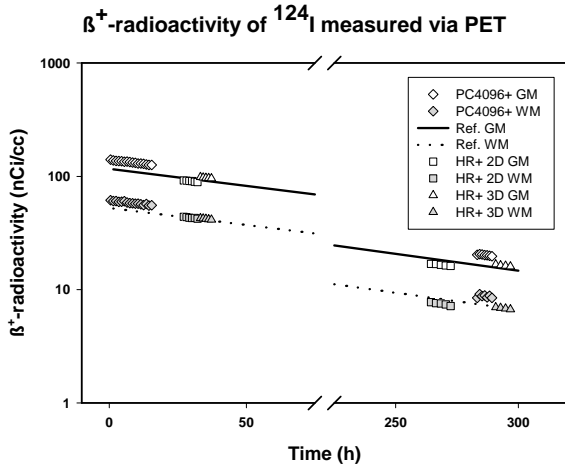
Fig. 4. Positron radioactivity measured by the PC4096+ and the HR+ scanners in studies S2A and S2B. The reference data were obtained from γ-ray spectroscopy.

Table 2
Relative differences (%) of radioactivity determined by PET in respect of the measurement by γ-ray spectroscopy[a]

			S1A	S1B	S2A	S2B	[18]F
PC4096+			−4.1	−4.1	20.3	25.1	9.5
HR+	2D	CPU	−20.4	−18.9	−4.4	−9.4	−8.4
		VP	−19.6	−16.8	−4.3	−7.4	−6.8
	3D	CPU	−16.1	−14.3	6.2	6.6	4.9
		VP	−24.4	−22.3	−4.0	−4.1	−1.3

[a] For ^{18}F the relative differences are with respect to values measured with a curiemeter.

greater ratio with the late scans (S1B and S2B). Using the HR+ the ratio was always smaller in 2D compared to 3D. For the S1 studies all ratios determined with the HR+ decreased from the early to the late scan—in contrast to the PC4096+. The equivalent data increased in the S2 studies for all HR+ conditions—in agreement with the PC4096+. For purpose of comparison, Table 3 also contains GM/WM ratios resulting from equivalent ^{18}F studies.

Table 3
Ratios of the radioactivity concentrations in grey and white matter chamber (GM/WM ratios)

			S1A	S1B	S2A	S2B	[18]F
Real			3.10		2.21		2.81
PC4096+			3.01	3.09	2.28	2.32	2.89
HR+	2D	CPU	2.90	2.68	2.10	2.21	2.76
		VP	2.84	2.60	2.13	2.17	2.69
	3D	CPU	3.16	3.03	2.30	2.39	3.11
		VP	3.24	3.06	2.34	2.44	2.87
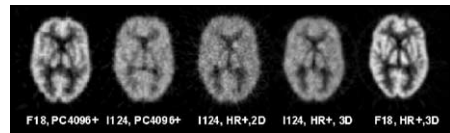
Fig. 5. Transversal slices of 3D-Hoffman-phantom filled with either [124]I or [18]F. The scans were taken with the PC4096+, and the HR+ in 2D- and 3D-mode.

Fig. 5 shows the reconstructed images of the 3D-Hoffman phantom. Here, the increased background present in the [124]I scans in comparison to the ^{18}F scans becomes evident. The HR+-scans of [124]I clearly demonstrated the increased signal/noise ratio in the 3D-mode.

4. Discussion

This report presents a number of tests by which the quantitative and imaging performance of the non-pure positron emitter [124]I was assessed. Only 23% of the radioactive decays represent positron emission. All other counts do not contribute to the PET signal, but may impair the quality as well as the accuracy of the reconstructed PET images. There are single photons of energies 602 and 722 keV with abundances of 61% and 10%, respectively. Although the 722 keV photons are above the energy window ranging from 350 to 650 keV, they may have some minor influence after loss of energy by scattering so that they are accepted within the energy window. Half of the single photons just increase the number of random coincidences which should be corrected for by the routinely available correction procedures. 50% of the 602 keV photons are emitted simultaneously with positrons possibly producing gamma coincidences which become visible as a uniform distribution when the capillary was in air (Figs. 2a and b). When the line source was located in water the

background was no longer uniform, but decreased with a greater radius due to scattering (Figs. 2c and d). Gamma coincidences are of course more present in the 3D- than in the 2D-acquisition mode as shown in Figs. 2 and 3. Non-true coincidences also affect the images of the Hoffman phantom where they cause an increased background and a loss of contrast (Fig. 5). This loss of contrast may be augmented to some extent by the slightly worse image resolution which is related to the higher positron range of ^{124}I than that of ^{18}F. The 602 keV photons emitted simultaneously with positrons may also yield multiple coincidences—especially in 3D—if such a photon hits the detector ring together with both the annihilation photons. Such multiple coincidences are rejected by the detector electronics so that the true information contained in the pair of the 511 keV photons is lost. On the other hand, the chance of such multiple coincidences is rather low.

In spite of the gamma coincidences, which are not corrected by any of the preprocessing software of the two scanners, the outcome of the absolute radioactivity concentration is in general lower than the positron activity values measured by γ-ray spectroscopy. When the 2D-behaviour of the scanner hardware is compared, less gamma coincidences can be expected for the PC4096+ than for the HR+, because the PC4096+ has more extended septa and a smaller acceptance angle per detector ring. This fact is in concordance with the known higher scatter fraction of the HR+-2D-mode and also with the line-profiles presented in Fig. 3. When going from the 2D- to 3D-mode of the HR+, Fig. 2. confirms another expected increase of background by gamma coincidences. In spite of this increase, the absolute activity concentration obtained in the 3D scans is not greater than the 2D findings when the VP-reconstruction was selected. Only for the CPU reconstruction the reconstructed absolute radioactivity concentration is greater. However, as this is also true for the ^{18}F data (Table 2), this effect is probably not caused by more recorded gamma coincidences. Although the sinograms of the line sources as well as that of the two-chamber phantom show an increased background outside the radioactivity source, the reconstructed images do not reveal such an increased background with values of <1% of the GM results. With these statements in mind, the differences present in Table 2 are obviously caused more by systematic differences in the reconstruction software, e.g. CPU vs. VP reconstruction mode, by inaccurate calibration, and finally possibly by residual errors in the γ-ray spectroscopy.

Dependent on the individual mode of measurement, over- and underestimations of the true GM/WM ratio were found. This is also true for ^{18}F, so that here no specific effect can be attributed to ^{124}I. Although different checks were made, it remains unclear why the GM/WM ratio determined with HR+ in 2D and 3D decreases from S1A to S1B, whereas it increases from S2A to S2B. A possible explanation may be that the events collected during S1A are much lower than those in S2B, with the consequence of errors related to poor counting statistics. Another reason of such a discrepancy could be the presence of impurities produced together with the ^{124}I-activity which would differ between the two study series S1 and S2. This is, however, not probable because a standardized production procedure was used which had been validated with regard to the purity of ^{124}I (Bastian et al., 2001). Furthermore, the half-lives derived from the measured data differed only slightly from the known half-life of ^{124}I. So there was no indication of an impurity.

There is yet another possible problem in the use of non-pure positron emitters. The additional non-annihilation photons are seen by the scintillation detector, even if they do not fall within the energy window, and contribute to the detector dead-time. (Lubberink et al., 2001). On the other hand, our observation on the half-life described above does not indicate any problem with the dead-time.

The data reconstructed here utilized "warm" transmission scans. This is a situation which may be common for patient studies. The comparative application of "cold" transmission scans indicated that the "true" radioactivity values are higher by 2–4% in the case of brain scans. This difference would be greater in whole-body studies.

The measurements described here support the feasibility of quantitative PET studies with ^{124}I although the available PET systems do not yet supply a correction for the additional gamma coincidences. Our results indicate that errors introduced by these coincidences are within the errors of calibration associated with daily routine studies. However, one definite conclusion of this study is that these errors must be decreased by a stricter quality control of the analytical procedures. If this is achieved, the correction procedures may be further optimized for the use of non-pure positron emitters such as ^{124}I.

References

Bastian, T.H., Coenen, H.H., Qaim, S.M., 2001. Excitation functions of ^{124}Te(d, *x*n) ^{124,125}I reactions from threshold up to 14 MeV: comparative evaluation of nuclear routes for the production of ^{124}I. Appl. Radiat. Isot. 55, 303–308.

Bergström, M., Eriksson, L., Bohm, C., Blomqvist, G., Litton, J., 1983. Correction for scattered radiation in a ring detector positron camera by integral transformation of the projections. J. Comput. Assist. Tomogr. 7, 42–50.

Brix, G., Zaers, J., Adam, L., Bellemann, M.E., Ostertag, H., Trojan, H., Haberkorn, U., Doll, J., Oberdorfer, F., Lorenz, W.J., 1997. Performance evaluation of a whole-body PET scanner using the NEMA protocol. J. Nucl. Med. 38, 1614–1623.

Carnochan, P., Trivedi, M., Young, H., Eccles, S., Potter, G., Haynes, B., Ott, R., 1994. Biodistribution and kinetics of radiolabelled pyrrolidino-4-iodo-tamoxifen: prospects for pharmacokinetic studies using PET. J. Nucl. Biol. Med. 38 (Suppl. 1), 96–98.

Coenen, H.H., Dutschka, K., Muller, S.P., Geworski, L., Farahati, J., Reiners, C., 1995. N.c.a. radiosynthesis of [^{123,124}I]beta-CIT plasma analysis and pharmacokinetic studies with SPECT and PET. Nucl. Med. Biol. 22, 977–984.

Defrise, M., Townsend, D.W., Clark, R., 1989. Three-dimensional image reconstruction from complete projections. Phys. Med. Biol. 34, 573–583.

Defrise, M., Kinahan, P.E., Townsend, D.W., Michel, C., Sibomana, M., Newport, D.F., 1997. Exact and approximate rebinning algorithms for 3-D PET data. IEEE Trans. Med. Imag. 16, 145–158.

Langen, K.J., Coenen, H.H., Roosen, N., Kling, P., Muzik, O., Herzog, H., Kuwert, T., Stöcklin, G., Feinendegen, L.E., 1990. SPECT studies of brain tumors with L-[^{123}I]iodo-methyl-tyrosine (^{123}IMT): first clinical results and comparison with PET and ^{124}IMT. J. Nucl. Med. 31, 281–286.

Lubberink, M., Schneider, H., Bergström, M., Lundqvist, H., 2001. Count rate characteristics of PET with bromine-76. Eur. J. Nucl. Med. 28, 1008.

Pentlow, K.S., Graham, M.C., Lambrecht, R.M., Daghighian, F., Bacharach, S.L., Bendriem, B., Finn, R.D., Jordan, K., Kalaigian, H., Karp, J.S., Robeson, W.R., Larson, S.M., 1996. Quantitative imaging of iodine-124 with PET. J. Nucl. Med. 37, 1557–1562.

Qaim, S.M., Blessing, G., Tárkányi, F., Lavi, N., Bräutigam, W., Scholten, B., Stöcklin, G., 1996. Production of lover-lived positron emitters ^{73}Se, ^{82m}Rb and ^{124}I. In: Cornell, J.C., (Ed.), Proceedings of the 14th International Conference on cyclotrons and their Applications, Cape Town, South Africa, October 1995. World Scientific, Singapore, p. 541.

ICRP Publication 38, 1983. Radionuclide transformations, energy and intensity of emissions. Annals of the, ICRP, Pergamon Press, Oxford.

Rota Kops, E., Herzog, H., Schmid, A., Holte, S., Feinendegen, L.E., 1990. Performance characteristics of an eight-ring whole-body PET scanner. J. Assist. Comput. Tomogr. 14, 437–445.

Scholten, B., Kovács, Z., Tárkányi, F., Qaim, S.M., 1995. Excitation functions of ^{124}Te(p,n) ^{124,123}I reactions from 6 to 31 MeV with special reference to the production of ^{124}I at a small cyclotron. Appl. Radiat. Isot. 46, 255–259.

Watson, C.C., 2000. New, faster, image-based scatter correction for 3D PET. IEEE Trans. Nucl. Sci. 47, 1587–1594.

Watson, C.C., Newport, D., Casey, M.E., deKemp, R.A., Beanlands, R.S., Schmand, M., 1997. Evaluation of simulation-based scatter correction for 3-D PET cardiac imaging. IEEE Trans. Nucl. Sci. 44, 90–97.